José Risso

Alberto Cardona
e-mail: acardona@intec.unl.edu.ar

Andres Anca

CIMEC - INTEC (UNL/Conicet),
Güemes 3450,
(3000) Santa Fe,
Argentina

Violeta Colpachi
Research & Development,
Fundición San Cayetano,
L.M. Drago y Melián,
1852 Burzaco,
Argentina

Computation of Stress and Strain Evolution During Heat Treatment of Work Rolls

We present a numerical simulation of heat treatment of cast metallic alloys by the finite element method, to predict strains and stresses produced during the said process. From a computational point of view, this problem involves a coupled thermal-metallurgical-mechanical analysis modeled as a non-stationary and non-linear process. The calculation of metallurgical properties is coupled directly with thermal analysis. Material properties, which are dependent on temperature and microstructural composition, are rewritten for the purpose of the analysis as functions of temperature and time. Results of thermo-metallurgical analysis are taken as data for the subsequent mechanical analysis. The simulation was successful and proved the causes of failure during heat treatment of a centrifugally cast three-layered Hi-Chrome work roll. [DOI: 10.1115/1.2198247]

1 Introduction

Heat treatment of metallic alloys is a complex thermomechanical process involving solid state metallurgical transformations that change both the thermal and the mechanical properties of materials. This process is widely used in industrial applications to release internal stresses, reduce fragility, improve machinability, or modify properties like hardness or strength to satisfy the requirements of a definite application. However, a badly designed heat treatment can cause undesirable strains and stresses, and also cracking. This fact must be taken into account when designing the heating and cooling sequences in the process.

Numerical simulation of heat treatment has been the subject of much research work focusing either on thermal and mechanical analysis of the process [1–4] or on aspects of material modeling [5–8].

Material models capable of accounting for variations in thermal and mechanical properties due to temperature and metallurgical structure changes are a key point to simulate the thermomechanical evolution of parts subjected to heat treatment. A first type of models exists that describe the microstructure evolution as a function of alloy composition, temperature, and cooling time, reproducing either isothermal (TTT) or continuous cooling (CCT) diagrams for different alloys and chemical compositions [9–14]. Once the microstructure is known, a second type of model describes material properties as functions of microstructure, alloy composition, and temperature [7,8]. Using models of both types, we can predict the material properties needed for thermomechanical computations.

The latter procedure is useful to develop material models for a broad range of well-known alloys (carbon and low-alloy steels, austenitic stainless steels, etc.). However, as Taleb points out [15], its effectiveness is very limited for special alloys (e.g., for high-alloy white iron) since the model obtained is not able to represent with accuracy the material properties observed experimentally. Taleb proposed several corrections to the standard models to reproduce material properties in the alloys he modeled.

In this work, we follow an alternative way to represent material properties for heat treatment simulation. We redefined material properties as functions of time and temperature, by merging TTT/CCT diagrams with curves of dependency of thermo-mechanical properties in terms of temperature and metallurgical composition a priori. In this way, material properties were represented by piecewise linear interpolation of the final properties observed in experiments in terms of time and temperature. The simulations were done using a commercial finite element software which takes into account the dependence of material properties on time and temperature [16].

Section 2.1 describes the numerical model used to simulate thermo-mechanical processes in heat treatment of ferrous metals. In Sec. 2.2, a description of the proposed material model is given. Section 3 presents an application of this model to the simulation of the heat treatment of centrifugally cast three-layered Hi-Chrome work rolls, commonly used in steel mills. The simulation accounted for and reproduced the kind of actual failures observed during heat treatment of these types of work rolls.

2 Numerical Model

2.1 Thermomechanical Model. The numerical analysis of heat treatment processes can be made by modeling the time evolution of two coupled problems:

- A thermal problem which involves heating and cooling of parts and must take into account the variations of material properties (thermal conductivity and enthalpy) caused by temperature and microstructural transformations as well as heat releasing/absorption phenomena (related to latent heat), during metallurgical transformations.
- A mechanical problem which arises when it comes to predicting stresses and strains generated by thermal expansion/contraction produced by temperature changes and also by metallurgical phase transformations.

The thermal problem is nonlinear because material parameters depend on temperature. The mechanical problem is also nonlinear because thermal and transformation-induced strains often generate plastic deformations.

Provided there are no strong mechanical perturbations that could induce metallurgical transformations (e.g., transformation of retained austenite to martensite, induced by stresses generated by external loads), mechanical phenomena do not affect thermal

Contributed by the Applied Mechanics Division of ASME for publication in the JOURNAL OF APPLIED MECHANICS. Manuscript received September 27, 2005; final manuscript received January 3, 2006. Review conducted by G. C. Buscaglia. Discussion on the paper should be addressed to the Editor, Prof. Robert M. McMeeking, Journal of Applied Mechanics, Department of Mechanical and Environmental Engineering, University of California – Santa Barbara, Santa Barbara, CA 93106-5070, and will be accepted until four months after final publication in the paper itself in the ASME JOURNAL OF APPLIED MECHANICS.

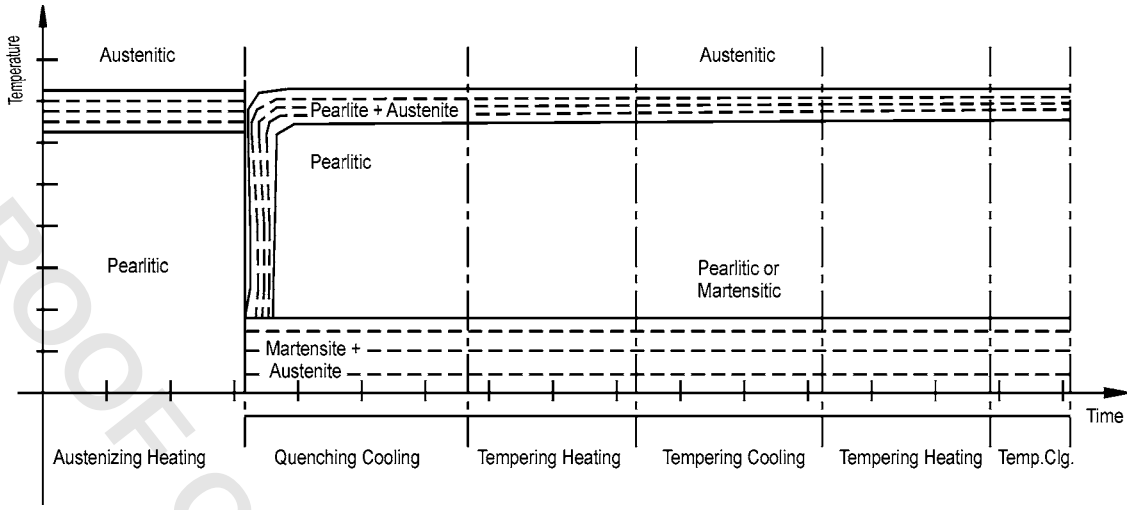

Fig. 1 Approximation of temperature-time transformation

properties. Under this assumption we can ignore the dependency of the thermal model on the mechanical variables, which enables us to perform an uncoupled thermal analysis followed by a mechanical analysis that takes the thermal results as input.

The differential equation describing the thermal problem is

$$\rho(T)\frac{\partial H(T,m)}{\partial t} - \nabla(k(T,m)\,\nabla\, T) = 0 \tag{1}$$

where ρ is the density, H the enthalpy, t is the time, k the conductivity, T the temperature, and m accounts for the dependency of material parameters on microstructure.

By assuming both phases have the same density, the relationship between capacity and enthalpy in the presence of phase change is given by the following expression

$$\begin{aligned}\rho(T)H(T,m) &= \int_A^B \rho(T)c_{\text{eff}}(T,m)dT \\ &= \int_A^{\text{epc}} \varphi_1(T)\rho(T)c_1(T)dT + \rho(T)L_{pc} \\ &\quad + \int_{\text{spc}}^B \varphi_2(T)\rho(T)c_2(T)dT \end{aligned} \tag{2}$$

where c_{eff} is the effective (apparent) heat capacity, c_1 and c_2 are the specific heats for different microstructures, φ_1 and φ_2 are the fractions of initial and final microstructural components, L_{pc} is the latent heat necessary for a phase change, spc is the initial temperature of phase change, and epc the temperature at the end of phase change.

The dependence of the thermal problem on metallurgical transformations is simulated with an enthalpy model that takes into account heat capacity of metal, and latent heat exchange occurring during phase changes.

The dependence of the mechanical properties on material microstructure is simulated using material models that account for variations in metallurgical constituents with time. The thermal dependence of the mechanical problem is modeled using a temperature field calculated in the thermal simulation and given as input to evaluate the mechanical properties for the mechanical analysis and to compute the strains.

In the mechanical simulation, we use a classic elastoplastic model with isotropic hardening, in which the stresses are calculated as

$$\boldsymbol{\sigma} = \mathbf{C}(T,\varepsilon_p,m)\boldsymbol{\varepsilon}_e = \mathbf{C}(T,\varepsilon_p,m)(\boldsymbol{\varepsilon} - \boldsymbol{\varepsilon}_p - \boldsymbol{\varepsilon}_t), \tag{3}$$

where $\boldsymbol{\sigma}$ and $\boldsymbol{\varepsilon}$ are stress and strain vectors, $\mathbf{C}$ is the constitutive tensor, $\boldsymbol{\varepsilon}_\mathbf{e}$ is the elastic strain, $\boldsymbol{\varepsilon}_\mathbf{p}$ is the plastic strain, and $\boldsymbol{\varepsilon}_\mathbf{t}$ is the thermal-microstructural strain, which integrates the effect of thermal expansion and volume variations during metallurgical phase

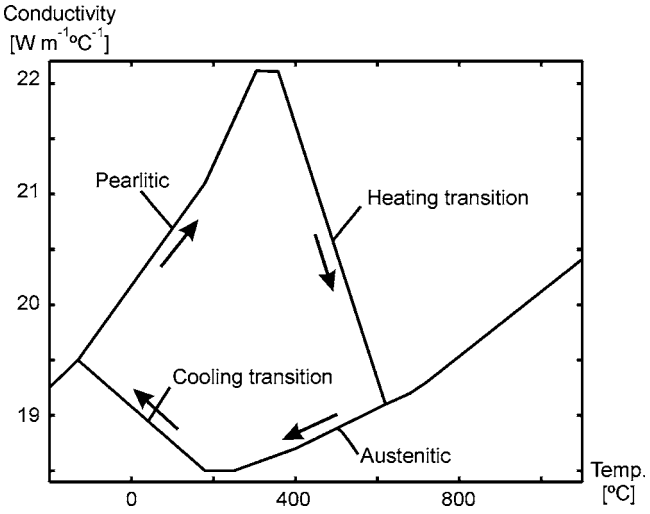

Fig. 2 Conductivity versus temperature approximation

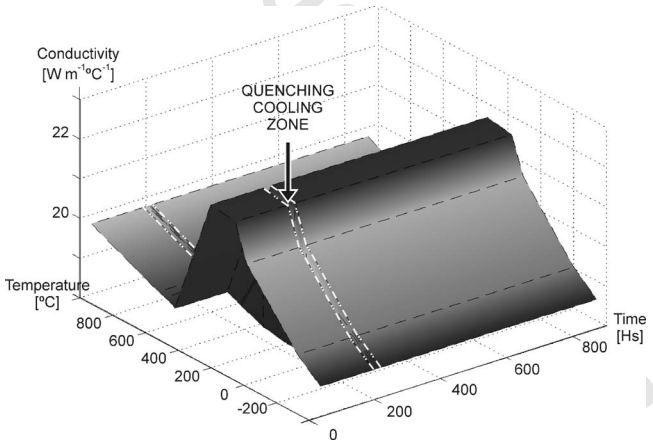

Fig. 3 Conductivity versus time/temperature diagram

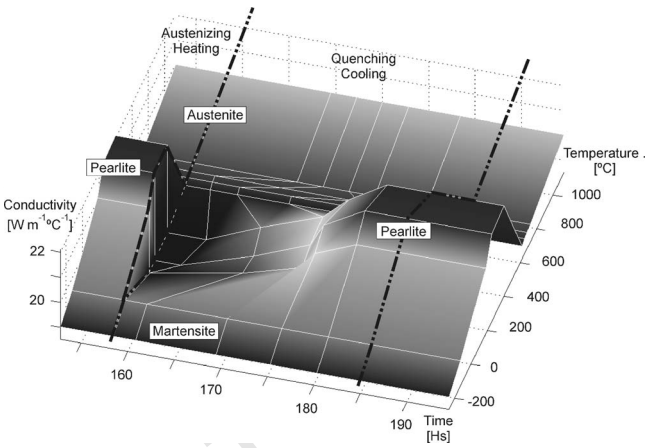

Fig. 4 Conductivity versus time/temperature diagram—detail in the quenching cooling zone

changes.

The stress field must satisfy a yield criterion (in this case, the isotropic Von Mises criterion)

$$\sigma_{eq} = \sqrt{\frac{1}{2}[(\sigma_x - \sigma_y)^2 + (\sigma_y - \sigma_z)^2 + (\sigma_z - \sigma_y)^2 + 6(\tau_{xy}^2 + \tau_{yz}^2 + \tau_{zx}^2)]}$$

$$\leqslant Y(T, \varepsilon_{eq}, m) \tag{4}$$

Since the limit stress Y is a function of the temperature, of the equivalent plastic strain ε_{eq} and of the microstructure, the model can take into account the variation of material hardening behavior with temperature.

2.2 Material Model. Most material properties are functions of temperature and microstructure, and therefore have indirect dependency on variables such as time and maximum heating/cooling temperature which define material microstructure.

In austenizing processes (heating), the microstructure is modeled as a function of temperature only. In quenching processes (cooling), the microstructure is a function of temperature and time. In tempering processes (heating and cooling) the microstructure is considered as a function of temperature only (the dependency upon temperature and time could be modeled if data about transformations of retained austenite were available).

Then, for the whole process, we can formulate any general property μ as a function of temperature and time, as follows

$$\mu = \mu[T, m(T,t)] = \mu(T,t) \tag{5}$$

In order to define the material parameters, we first construct a map of microstructure as a function of temperature and time using data about heating and cooling periods, and isothermal (TTT) or continuous cooling (CCT) diagrams for the quenching cooling interval, as shown in Fig. 1. Then, for every definite material microstructure (i.e., austenitic, pearlitic, martensitic), we define the value of every property as a function of temperature. Figure 2 is an example for the case of conductivity. Finally, by combining the map of microstructure as a function of temperature and time with the curves of temperature dependence of the considered

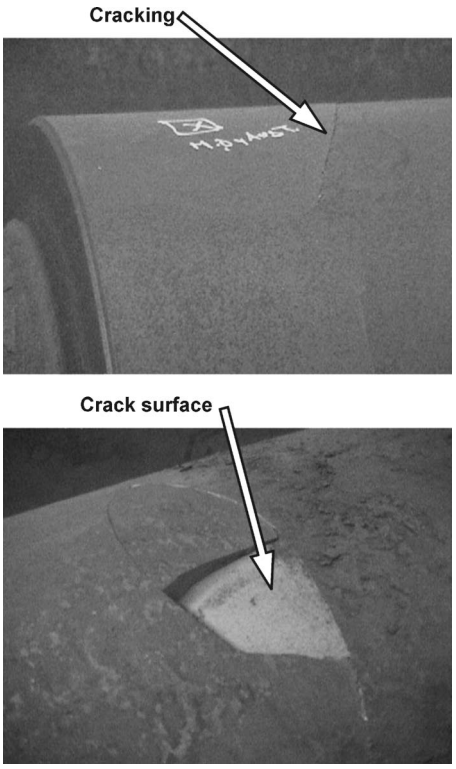

Fig. 6 Observed cracks in the barrel of work rolls

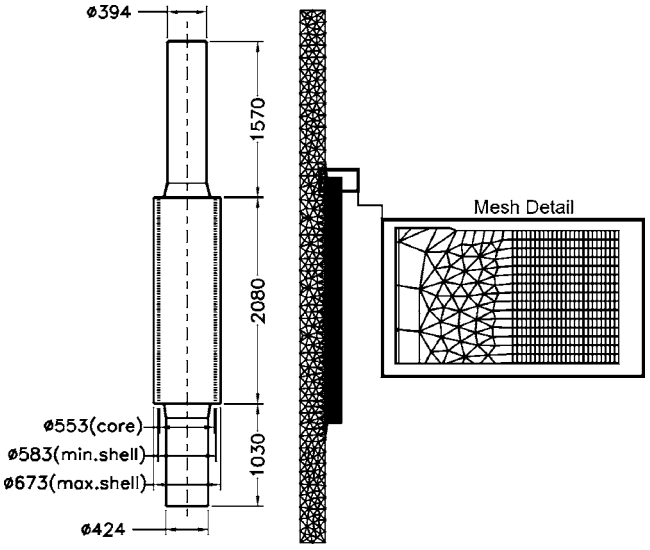

Fig. 5 (Left) Work roll main dimensions, (right) FEM mesh

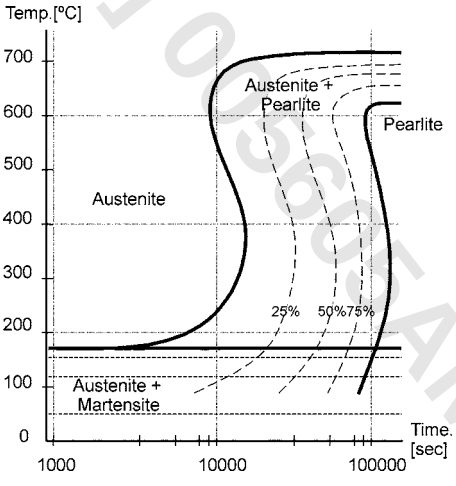

Fig. 7 Temperature-time-transformation diagram for Hi-Cr iron (shell)

Table 1 Convective boundary condition. Time variation of air temperature and heat transfer coefficients (intermediate values calculated by linear interpolation).

Time [s]	Temp. [°C]	Time [s]	Temp. [°C]	Time [s]	Heat transfer coefficient [W m^{-2} °C^{-1}]
0	25	1,590,000	520	0	40
160,000	170	1,620,000	490	<570,000	40
175,000	180	1,675,500	480	570,000	30
290,000	430	1,676,000	80	577,000	50
320,000	420	1,713,300	30	585,000	40
380,000	780	2,200,000	55	585,100	60
381,000	730	2,225,000	65	588,000	65
419,000	680	2,247,000	80	589,000	36
428,000	880	2,265,000	85	595,000	10
430,000	1080	2,311,600	160	599,000	15
440,000	1060	2,330,000	165	600,000	8
481,000	1090	2,380,000	310	613,000	12
500,000	1040	2,410,000	310	615,000	4
<570,000	1020	2,450,000	410	900,000	3
570,000	80	2,473,600	410	1,200,000	3
577,000	30	2,500,000	530	1,275,600	40
600,000	30	2,530,000	510	1,675,500	40
600,100	520	2,550,000	555	1,676,000	10
665,000	520	2,610,000	530	1,705,000	10
665,100	30	2,630,000	570	1,706,000	3
1,200,000	25	2,675,200	540	2,200,000	3
1,275,600	100	2,675,300	30	2,225,000	40
1,297,200	95	2,815,600	30	2,675,200	40
1,394,400	205	2,819,200	60	2,675,300	10
1,416,000	205	2,862,400	60	2,804,800	10
1,545,600	465	2,873,200	30	2,815,500	3
1,556,400	430			2,873,200	3

property, and by using the rule of mixtures for regions with mixed structure (e.g., austenite+pearlite), a map of the property as a function of temperature and time (continuous piecewise linear approximation) can be built, as shown in Fig. 3.

We used a commercial finite element code in which material properties can be defined as functions of temperature and time [16]. When using such a standard material model, special care must be taken to adapt the map of microstructure as a function of temperature and time to the real quenching cooling process (see Fig. 4) to avoid reversions in austenite-pearlite and austenite-martensite transformations. An improvement currently in progress is the development of a model with the ability to track microstructural evolution and avoid numerical reversion of physically irreversible phase changes.

In the thermal analysis, the material parameters are the enthalpy and the thermal conductivity. In the mechanical analysis, the material parameters are the Young (elastic) modulus, the Poisson coefficient, the thermal expansion coefficient, and the yield stress. All of them are modeled following the above-mentioned procedure to account for variations during the heat treatment process.

3 Application Case

3.1 Problem Description. The Hi-Chrome work rolls used in the initial stages of steel lamination have an exterior layer (shell) of Hi-Chrome white iron, an intermediate layer of low-alloy iron, and a core of spheroidal graphite iron. The first two layers are cast centrifugally in horizontal position, and afterwards the core is poured statically in vertical position. Typical as-cast dimensions are shown in Fig. 5.

After casting, rolls are heated from room temperature to 1020 °C (with complete austenitization). Then, they are quenched by cooling in air at room temperature. Finally, they are subjected to two tempering processes at 480 and 540 °C, each one followed by a slow cooling in air to room temperature.

After heat treatment, some rolls showed cracks near the corners of the barrel. In all cases the cracks had conic shape, starting at the end of the barrel in the vicinity of the interface between Hi-Chrome and interface layers, and ending at the external diameter of the barrel, approximately 250 mm away from the barrel's edge, as shown in Fig. 6.

Even though circumferential cracks in the external diameter of the roll were observed several hours after the end of the second tempering, when rolls were already at room temperature, the presence of black ferrous oxides in the initial zone of the cracks indicated that the cracking started in an intermediate stage of the heat treatment (at least previously to the last tempering heating). The aim of this analysis was to determine the stage where cracking

Table 2 Properties for Hi-Cr iron (shell) in austenitic state

Temperature [°C]	Enthalpy [J kg^{-1}]	Conductivity [W m^{-1} °C^{-1}]	Young's modulus [Pa]	Secant thermal expansion coefficient [°C^{-1}]
180	0.62E5	18.50	2.07E11	−2.60E-5
250	1.06E5	18.50	2.04E11	−1.00E-5
400	2.11E5	18.60	1.95E11	0.23E-5
620	3.87E5	19.00	1.74E11	0.95E-5
650	4.11E5	19.07	1.69E11	1.01E-5
680	4.40E5	19.12	1.65E11	1.07E-5
720	5.25E5	19.20	1.62E11	1.13E-5
1030	7.91E5	20.00	0.75E11	1.90E-5

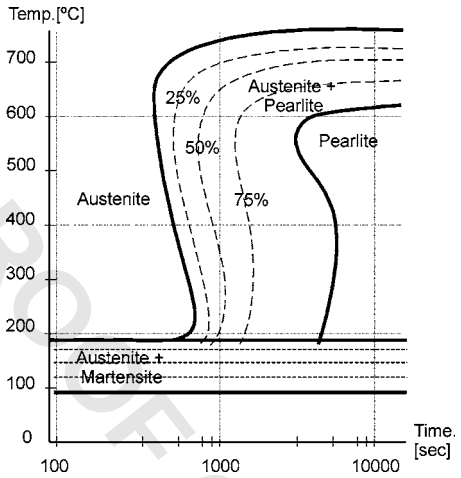

Fig. 8 Temperature-time-transformation diagram for SG iron (core)

starts, and to confirm the presence of residual stresses which may explain the advancement of the cracking front up to the external diameter of the barrel.

Ignoring small circumferential temperature differences and small bending stresses generated by the horizontal mounting of cylinders in the heater, the problem can be modeled as an axisymmetrical one. The finite element mesh, built by using axisymmetric triangular elements, is shown in Fig. 5(*b*). The same mesh is used for the thermal and the mechanical analyses. A quadratic interpolation of unknowns (i.e., temperatures and displacements, respectively) is used in both cases.

Convective boundary conditions were set on the external surface of the roll for the thermal analysis. Convection coefficients ranging from 5 to 40 W m^{-2} C^{-1} were used in the different stages of heating and cooling, depending on the agitation of surrounding air, as seen in Table 1. The temperature evolution of air is also displayed in this table.

3.2 Shell Material Data (Hi-Chrome White Cast Iron). The TTT diagram of a similar alloy was used to determine the position of the pearlitic nose [17]. The cooling behavior of the shell material was determined using data of Hi-Cr white iron without Ni [18], with a correction of the transformation time to take into account the influence of Ni and Mo as suggested by Laird et al. [19]. The diagram is shown in Fig. 7.

The thermal conductivity as a function of temperature and microstructure was taken from data for high-alloy white iron [17,20]. Enthalpy values were calculated integrating the effective thermal capacity data [17,20] along the temperature range covered in the process. In order to calculate thermal-metallurgical strains, a secant expansion coefficient averaged from values found in bibliography [18,20] and based on a reference state of pearlitic structure at 20°C was used.

The elastic modulus as a function of temperature and chemical

Table 3 Properties for Hi-Cr iron (shell) in pearlitic-bainitic state

Temperature [°C]	Enthalpy [J kg^{-1}]	Conductivity [W m^{-1} °C^{-1}]	Young's modulus [Pa]	Secant thermal expansion coefficient [°C^{-1}]
−130	0.0	19.00	2.18E11	0.80E-5
180	1.07E6	19.50	2.12E11	0.88E-5
250	1.51E6	21.10	2.09E11	0.98E-5
400	2.56E5	22.00	2.00E11	1.18E-5
620	4.32E5	22.10	1.79E11	1.30E-5

Table 4 Yield stress for Hi-Cr iron (shell)

Temperature [°C]	Yield stress (austenitic) [Pa]		Yield stress (pearl./bain.) [Pa]	
	ϵ_{eq}=0.0	ϵ_{eq}=0.1	ϵ_{eq}=0.0	ϵ_{eq}=0.1
0	…	…	8.0E+8	10.0E+8
100	…	…	7.0E+8	8.9E+8
300	4.3E+8	5.3E+8	5.0E+8	6.4E+8
620	2.4E+8	3.0E+8	2.6E+8	3.2E+8
650	2.2E+8	2.6E+8	…	…
680	1.9E+8	2.3E+8	…	…
720	1.6E+8	1.9E+8	…	…
1030	0.4E+8	0.5E+8	…	…

Table 5 Properties for gray iron (layer) in austenitic state

Temperature [°C]	Enthalpy [J kg^{-1}]	Conductivity [W m^{-1} °C^{-1}]	Young's modulus [Pa]	Secant thermal expansion coefficient [°C^{-1}]
190	0.28E5	29.80	1.12E+11	−2.10E-5
400	1.40E5	31.00	1.06E+11	0.26E-5
600	2.85E5	31.80	0.97E+11	0.94E-5
650	3.31E5	32.00	0.95E+11	1.01E-5
675	3.59E5	32.10	0.94E+11	1.07E-5
700	4.30E5	32.20	0.92E+11	1.10E-5
750	5.52E5	32.50	0.89E+11	1.17E-5
1030	8.01E5	37.00	0.44E+11	1.95E-5

Table 6 Properties for gray iron (layer) in pearlitic-bainitic state

Temperature [°C]	Enthalpy [J kg^{-1}]	Conductivity [W m^{-1} °C^{-1}]	Young's modulus [Pa]	Secant thermal expansion coefficient [°C^{-1}]
0	0.0	42.50	1.22E+11	1.22E-5
190	0.91E5	42.90	1.18E+11	1.28E-5
400	2.08E5	39.90	1.12E+11	1.35E-5
600	3.48E5	37.10	1.04E+11	1.39E-5
650	3.89E5	36.25	1.01E+11	1.42E-5

Table 7 Properties for SG iron (core) in austenitic state

Temperature [°C]	Enthalpy [J kg^{-1}]	Conductivity [W m^{-1} °C^{-1}]	Young's modulus [Pa]	Secant thermal expansion coefficient [°C^{-1}]
190	0.28E5	18.00	1.51E11	−1.90E-5
400	1.43E5	18.20	1.43E11	0.23E-5
600	2.91E5	18.60	1.32E11	0.91E-5
650	3.36E5	18.70	1.29E11	1.01E-5
675	3.65E5	18.75	1.27E11	1.06E-5
700	4.36E5	18.80	1.25E11	1.10E-5
750	5.57E5	18.95	1.20E11	1.17E-5
1030	8.05E5	20.00	0.60E11	1.95E-5

Table 8 Properties for SG Iron (core) in pearlitic-bainitic state

Temperature [°C]	Enthalpy [J kg^{-1}]	Conductivity [W m^{-1} °C^{-1}]	Young's modulus [Pa]	Secant thermal expansion coefficient [°C^{-1}]
0	0.0	39.00	1.65E11	1.06E-5
190	0.93E5	36.65	1.59E11	1.15E-5
400	2.12E5	29.85	1.51E11	1.30E-5
600	3.60E5	25.49	1.40E11	1.36E-5
650	4.04E5	25.00	1.36E11	1.38E-5

PROOF COPY [JAM-05-1355] 005605AMJ

Table 9 Yield stress for gray iron and SG iron (layer and core)

Temp. [°C]	Layer (austenitic) yield stress [Pa]		Layer (pearl./bain.) yield stress [Pa]		Core (austenitic) yield stress [Pa]		Core (pearl./bain.) yield stress [Pa]	
	ϵ_{eq}=0.0	ϵ_{eq}=0.1	ϵ_{eq}=0.0	ϵ_{eq}=0.1	ϵ_{eq}=0.0	ϵ_{eq}=0.1	ϵ_{eq}=0.0	ϵ_{eq}=0.1
0	…	…	6.60E+8	7.90E+8	…	…	7.00E+8	8.50E+8
100	…	…	6.20E+8	7.40E+8	…	…	6.50E+8	7.80E+8
300	4.30E+8	4.30E+8	4.50E+8	5.50E+8	4.50E+8	5.40E+8	4.80E+8	5.80E+8
620	1.60E+8	1.95E+8	1.70E+8	2.00E+8	1.80E+8	2.20E+8	1.90E+8	2.30E+8
650	1.50E+8	1.80E+8	…	…	1.70E+8	2.00E+8	…	…
680	1.30E+8	1.55E+8	…	…	1.45E+8	1.75E+8	…	…
720	0.97E+8	1.15E+8	…	…	1.10E+8	1.30E+8	…	…
1030	0.18E+8	0.22E+8	…	…	0.20E+8	0.25E+8	…	…

composition was obtained from data published by Belyakova et al. [19,21]. The Poisson coefficient was assumed constant and equal to 0.28. We assumed the yield stress dependence on temperature to be equal to that of the ultimate tensile stress for Hi-Cr white iron [19], scaled according to the room temperature yield stress of Hi-Cr. An isotropic hardening law was used.

Tables 2–4 show the values of these parameters in terms of temperature for austenitic and pearlitic/bainitic state. Data for material in martensitic state are not included because the evolution of temperatures during heat treatment of these rolls prevents the formation of martensitic structures.

3.3 Intermediate and Core Material Data (Gray and Spheroidal Graphite Cast Iron). Since the transformation curves of gray and spheroidal graphite cast iron are similar, the strategy used to determine their material parameters was the same for both. After determining the microstructure as a function of time and temperature, appropriate parameter values were selected. A TTT diagram for Ni-Mo ductile iron [22] was used to define the microstructure of the core material as a function of time and temperature in quenching. This diagram is shown in Fig. 8.

The thermal conductivity and the enthalpy as a function of heating and cooling temperature (obtained by integrating the apparent thermal capacity) were taken from data published by Auburn University researchers [23].

In order to compute thermal-metallurgical strains, a secant expansion coefficient based on a reference state of pearlitic structure at 20°C was calculated from tables of dilatometry in heating and cooling published by the Auburn Solidification Design Center

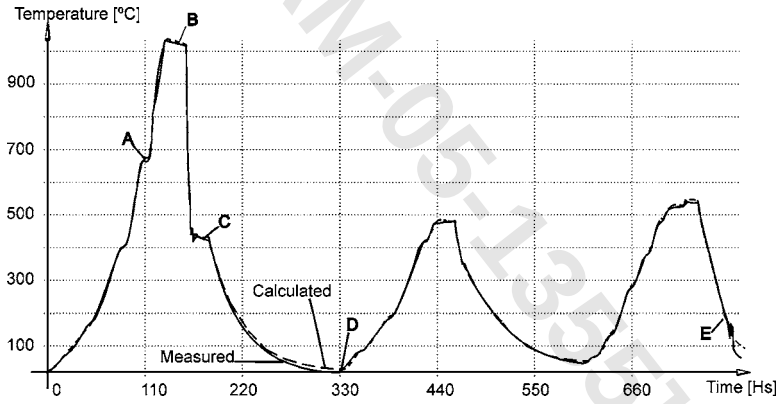

Fig. 9 Comparison between calculated and measured temperatures in barrel midpoint

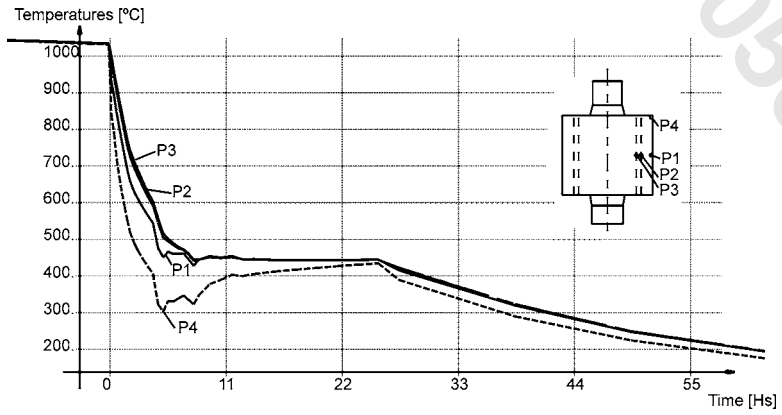

Fig. 10 Temperature evolution during quenching cooling

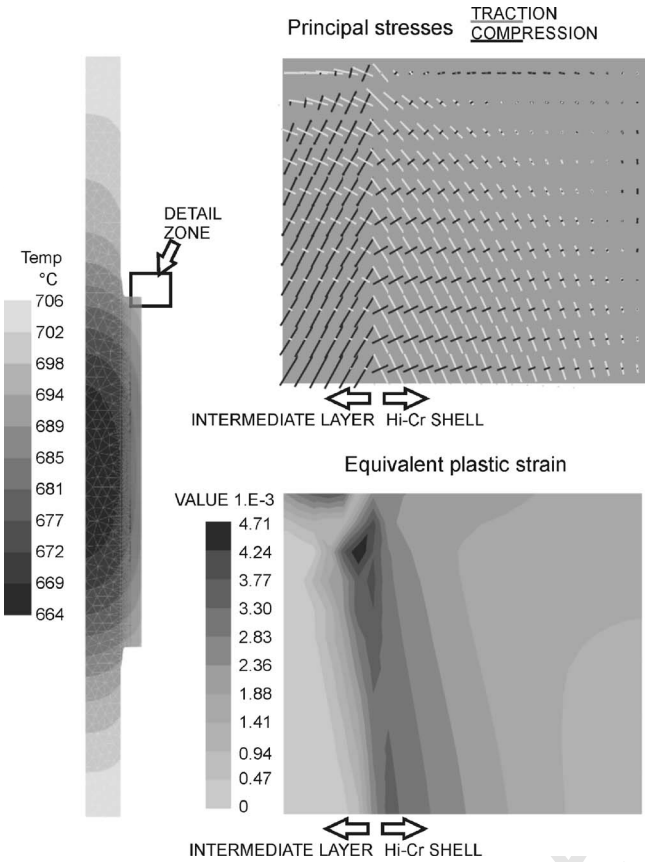

Fig. 11 Intermediate state during austenizing heating (point A, 110 h)

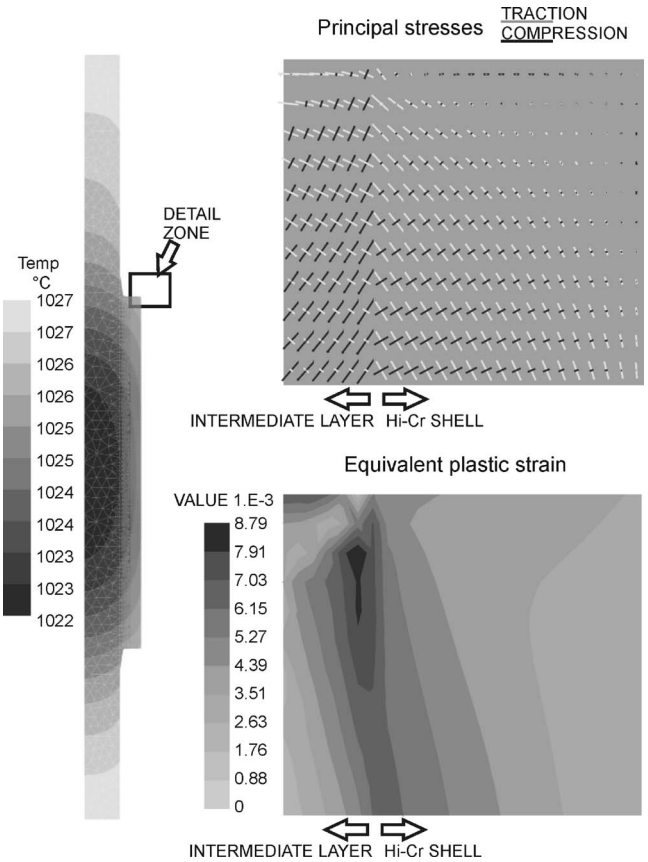

Fig. 12 End of austenizing heating (point B, 156 h)

[23]. The elastic modulus as a function of temperature was extrapolated from values at room temperature [17] and thermal dependency of this parameter for pearlitic steels. The Poisson coefficient was assumed constant and equal to 0.26. The yield stress dependence on temperature was taken from tables for gray and spheroidal graphite iron of similar composition [24].

Tables 5–9 show the values of these parameters as functions of temperature, for austenitic and pearlitic/bainitic state.

3.4 Results. A comparison between calculated (continuous line) and measured (dashed line) temperatures at the midpoint of the barrel surface is shown in Fig. 9. The agreement between curves is acceptable for the purposes of the analysis.

The largest differences between temperatures in different points of the roll, which define the maximum temperature gradients in the whole process, are found at the initial stage of quenching. Figure 10 shows a detail of the differences between points located in the surface of the barrel (P1, P4) and other points situated in the zones of transition between layers of different materials (P2, P3). The largest temperature difference predicted by computations between the surface and the core of the roll was lower than 300°C, and occurred during quenching.

The evolution of temperatures, principal stresses, and equivalent plastic deformations near the barrel corner, at the zone of failure, are shown in Figs. 11–15. These plots correspond to different time instants along the complete heat treatment, which were referred to by letters A–E in Fig. 9.

During the austenizing heating, tensile axial stresses develop in the external shell. However, as plastic deformations occur during heating, in the quenching and in the tempering processes the axial stresses in the shell become compressive. Moreover, large residual stresses develop and remain at the end of the process because of the differential deformation of core and layers.

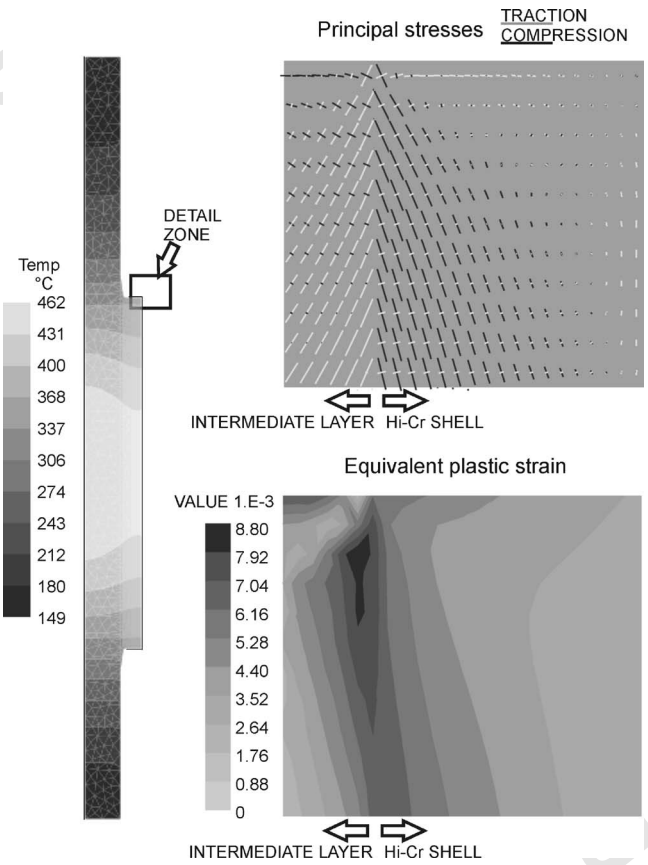

Fig. 13 Intermediate state during quenching cooling (point C, 166 h)

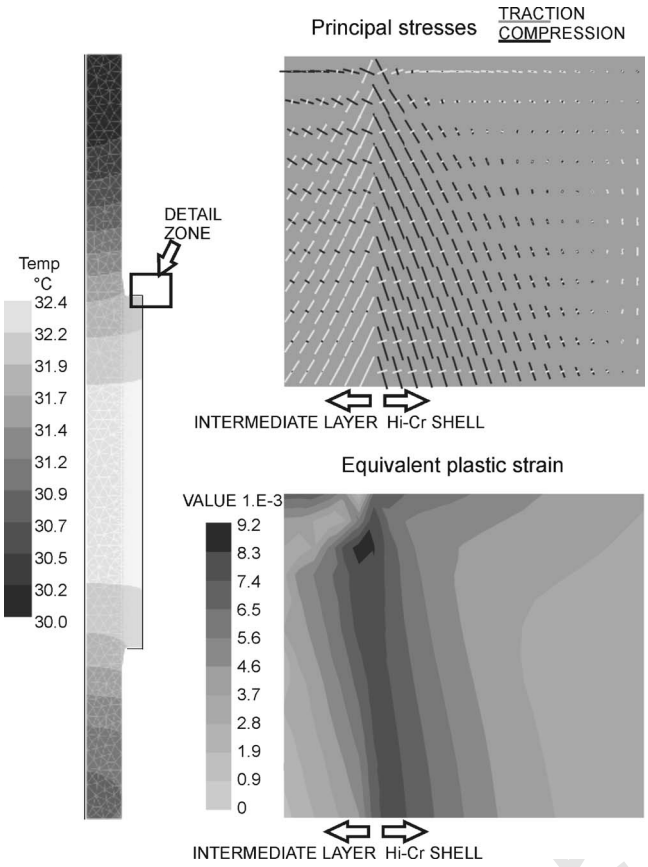

Fig. 14 End of quenching cooling (point D, 332 h)

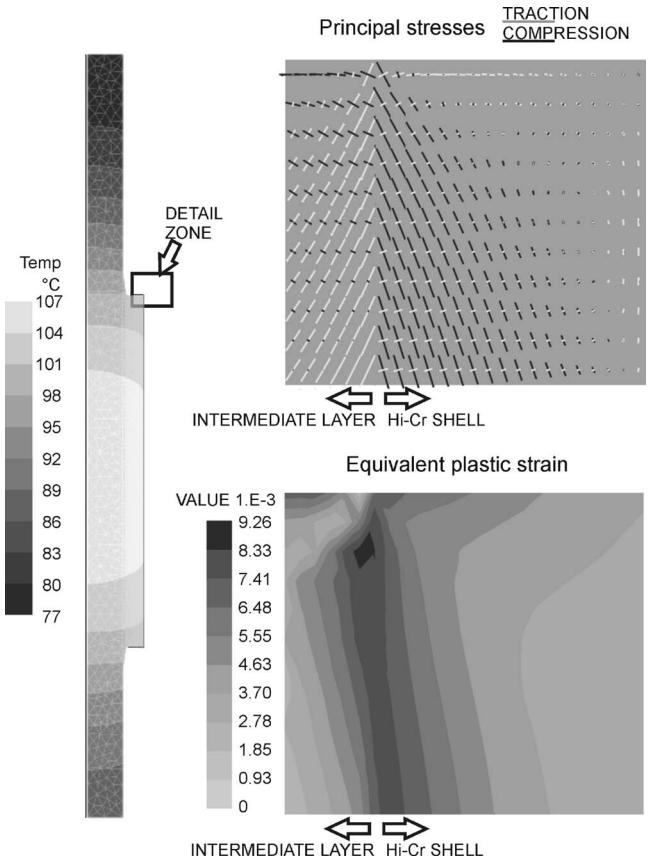

Fig. 15 End of second tempering cooling (point E, 792 h)

Figure 16 shows the evolution of equivalent plastic strains in different points near the barrel corner. Most inelastic deformations occur during the second half of the austenizing heating process and during the quenching process, as shown in the plots of evolution of equivalent plastic strain. Only a small increment in plastic strains is found during tempering processes. However, this result could be influenced by the lack of information about percentages of retained austenite after quenching and by transformations of retained austenite during tempering. The magnitude of inelastic strains found near the interface between shell and intermediate layers (close to 1%) is significant, specially if we take into account the brittle nature of Hi-Chrome white iron.

These two latter facts suggest that cracks started in the zone near the interface between shell and intermediate layers during the last stage of austenizing heating. The residual stresses observed at the end of the process (Fig. 15) are large enough to propagate these cracks in the plane perpendicular to the maximum tensile principal stresses up to the external surface of the barrel, in total coincidence with the observations (Fig. 6).

4 Conclusions

A model developed to simulate heat treatment of metals was presented. The approximation used to describe the behavior of thermo-mechanical variables, which was able to reproduce with accuracy the material properties observed experimentally, was found to be useful for special metal alloys. This type of parametrization allowed us to make an initial analysis with the small amount of data available in the literature for this special alloy. The analysis was very easily refined in regions of interest later on, when additional experimental data were obtained.

The main drawback of this approach is the need of knowing the approximate evolution of temperature in time a priori, in order to compute the resulting microstructure transformation at each point.

With regard to the analysis and design of work rolls, the results were of great aid in determining the causes of cracking failures and proposing preventive measures.

Finally, we should say that these results can be improved by using an initial stress field computed by an analysis of solidification in the casting process, and also by using data about the evolution of retained austenite in the shell material.

Acknowledgment

Financial support from Agencia Nacional de Promoción Científica y Tecnológica, Argentina, through Grant No. PID 99-76 and from Universidad Nacional del Litoral, through Grant No. CAI+D PE 214, is gratefully acknowledged.

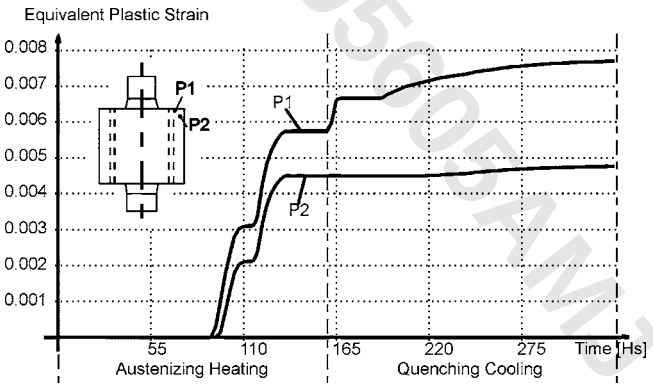

Fig. 16 Evolution of equivalent plastic strain

References

[1] Bergheau, J. M., Mangialenti, G., and Boitout, F., 1998, "Contribution of Numerical Simulation to the Analysis of Heat Treatment and Surface Hardening Processes," *Proc. of 18th ASM Heat Treating Conference and Exposition*, Wallis and Walton, eds., Rosemont, IL, p. 152.

[2] Aliaga, C., and Massoni, E., 1998, "3D Numerical Simulation of Thermo-Elasto-Visco-Plastic Behavior Using a Stabilized Mixed F.E. Formulation: Application to Heat Treatment," *Simulation of Materials Processing: Theory, Methods and Applications, Proc. Numiform'98*, Huétink and Baaijens, eds., Balkema, Rotterdam, The Netherlands, p. 263–269.

[3] Sanchez Sarmiento, G., Gastón, A., and Vega, J., 1998, "Inverse Heat Conduction Coupled With Phase Transformations Problems in Heat Treating Processes," *Computational Mechanics - New Trends and Applications*, Oñate and Idelsohn, eds., CIMNE, Barcelona, Spain, CD-Book Part VI, Sec. 1, paper 16.

[4] Berglund, D., 2001, "Simulation of Welding and Stress Relief Heat Treatment in Development of Aerospace Components," Licentiate thesis, Lulea University of Technology, Sweden.

[5] Kirkaldy, J., Thomson, B., and Baganis, E., 1978, "Hardenability Concepts With Applications to Steel," *AIME Transactions*, J. Kirkaldy and D. Doane, eds., Warrendale, PA, p. 82.

[6] Hömberg, D., 1996, "A Numerical Simulation of the Jominy End-Quench Test," Acta Mater., **44**(11), pp. 4375–4385.

[7] Alberg, H., 2003, "Material Modeling for Simulation of Heat Treatment," Licentiate thesis, Lulea University of Technology, Sweden.

[8] Saunders, N., Guo, Z., Li, X., Miodownik, A. P., and Schillé, J. P., 2003, "Using *JMatPro* to Model Materials Properties and Behavior," JOM, **55**(12), pp. 60–65.

[9] Johnson, W., and Mehl, R., 1939, "Reaction Kinetics in Processes of Nucleation and Growth," Trans. Am. Inst. Min., Metall. Pet. Eng., **135**, pp. 416–458.

[10] Lement, B. S., 1959, *Distortion in Tool Steels*, American Society for Metals, Metals Park, OH.

[11] Koistinen, D. P., and Marburger, R. E., 1959, "A General Equation Prescribing the Extent of the Austenite-Martensite Transformation in Pure Iron-Carbon Alloys and Plain Carbon Steels," Acta Metall., **7**, pp. 59–60.

[12] Leblond, J. B., Devaux, J., and Devaux, J. C., 1989, "Mathematical Modelling of Transformation Plasticity in Steels. I: Case of Ideal-Plastic Phases," Int. J. Plast., **5**, pp. 551–572.

[13] Leblond, J. B., 1989, "Mathematical Modelling of Transformation Plasticity in Steels. II: Coupling With Strain Hardening Phenomena," Int. J. Plast., **5**, pp. 573–591.

[14] Lusk, M., and Jou, H. H., 1997, "On the Rule of Additivity in Phase Transformation Kinetics," Metall. Mater. Trans. A, **28A**, pp. 287–291.

[15] Taleb, L., 2002, "Thermal, Metallurgical and Mechanical Interactions in the 16MND5 Steel," *Proc. of 1er Colloque interdisciplinaire sur les materiaux - Materiaux 2002*, Tours, France.

[16] Samtech, S. A., 2004, *Samcef/Mecano v10.1 User Manual*, Liege, Belgium.

[17] Betts, W., 2004 (personal communication).

[18] Gundlach, R., and Doane, D., 2003, "Alloy Cast Irons," *ASM Metals Handbook*, ASM International, Materials Park, OH, Vol. 1, pp. 85–104.

[19] Laird, G., Gundlach, R., and Rörig, K., 1996, "Heat Treatment of High-Alloy AR Cast Irons," *Abrasion-Resistant Cast Iron Handbook*, American Foundry Society, Schaumburg, IL, Chap. 3.

[20] Stefanescue, D., 1995, "Physical Properties of Cast Iron," *Iron Castings Engineering Handbook*, Blair et al., eds., ASM International, Materials Park, OH, pp. 223–244, Chap. 8.

[21] Belyakova, P. E., 1975, "Thermophysical Properties of Wear-Resisting Cast Irons," Metallovediene I Termicheskaya Obrabotka Metallov., **12**, pp. 45–48.

[22] Boyer, H., 1977, *Atlas of Isothermal Transformations and Cooling Transformations Diagrams*, ASM International, Materials Park, OH, pp. II–68.

[23] Wang, D., 2001, "Thermophysical Property Data," Auburn Solidification Design Center, http://metalcasting.auburn.edu/data/data.html

[24] Lynch, C. T., 1975, *CRC Handbook of Materials Science—Vol.2: Metals, Composites and Refractory Materials*, CRC, Boca Raton, FL.